THE JOURNAL OF PHYSICAL CHEMISTRY B

Article

pubs.acs.org/JPCB

Effect of Taiwan Mutation (D7H) on Structures of Amyloid-β Peptides: Replica Exchange Molecular Dynamics Study

Phan Minh Truong,[†,⊥] Man Hoang Viet,[‡,⊥] Phuong H. Nguyen,[§] Chin-Kun Hu,[∥] and Mai Suan Li*[,‡]

[†]Institute for Computational Science and Technology, SBI Building, Quang Trung Software City, Tan Chanh Hiep Ward, District 12, Ho Chi Minh City, Vietnam

[‡]Institute of Physics, Polish Academy of Sciences, Al. Lotnikow 32/46, 02-668 Warsaw, Poland

[§]Laboratoire de Biochimie Theorique, UPR 9080 CNRS, IBPC, Universite Paris 7, 13 rue Pierre et Marie Curie, 75005, Paris, France

[∥]Institute of Physics, Academia Sinica, Nankang, Taipei 11529, Taiwan

Supporting Information

ABSTRACT: Recent experiments have shown that the Taiwan mutation (D7H) slows the fibril formation of amyloid peptides Aβ_{40} and Aβ_{42}. Motivated by this finding, we have studied the influence of D7H mutation on structures of Aβ peptide monomers using the replica exchange molecular dynamics simulations with OPLS force field and implicit water model. Our study reveals that the mechanism behind modulation of aggregation rates is associated with decrease of β-content and dynamics of the salt bridge D23−K28. Estimating the bending free energy of this salt bridge, we have found that, in agreement with the experiments, the fibril formation rate of both peptides Aβ_{40} and Aβ_{42} is reduced about two times by mutation.

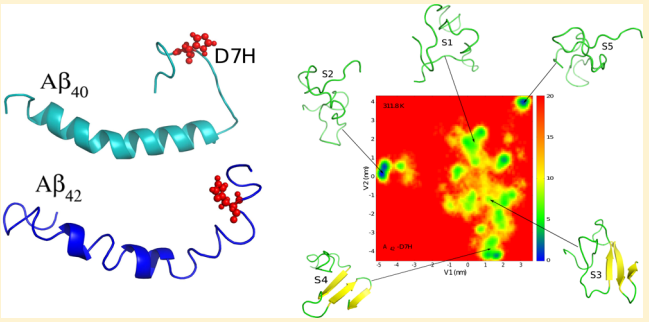

INTRODUCTION

Alzheimer's disease (AD) is the most common form of dementia among the senior population that is increasing substantially as populations age.[1] The patient with AD will lose memory,[2] experience language decay[3] and problems with visual−spatial search,[4] etc. AD may be pathologically characterized by progressive intracerebral accumulation of beta amyloid (Aβ) peptides[5] and tau protein.[6] However, recent genetic and pathological evidence strongly supported the first hypothesis.[7,8] The Aβ peptides are proteolytic byproducts of the amyloid precursor protein and are most commonly composed of 40 (Aβ_{1-40}) and 42 (Aβ_{1-42}) amino acids. Aβ peptides appear to be unstructured in the monomer state but aggregate to form fibrils with an ordered cross-β-sheet pattern.[9−12]

Increasing evidence from recent studies indicate that soluble oligomers are most neurotoxic,[5,13−15] while mature fibrils may be not toxic. The aesthetic of the cerebral defects in AD correlates with levels of oligomers in the brain, not the total Aβ stress.[16,17] Thus, the precise mechanism of toxicity of amyloid aggregates is not fully elucidated; however, there is evidence that prevention or reversion of the amyloid aggregation is beneficial. On the other hand, it is well-known that mutations can alter the toxicity, assembly, and rate of fibril formation of Aβ peptides. Because the turn region 21−23 of Aβ peptides might play a crucial step in fibril formation, numerous experimental[18−23] as well as theoretical[24−31] studies have been performed for various mutations in this region including the Flemish (A21G), Dutch (E22Q), Italian (E22K), Arctic (E22G), Iowa (D23N), and Osaka (ΔE22, deletion) variants. The G25L, G29L, G33L, G33A, G33I and G37L mutants of Aβ_{42} undergo β-sheet and fibril formation at an increased rate compared with wild-type (WT) Aβ_{42}.[32−35] On the other hand, as the region 1−8 of Aβ_{40} and 1−16 of Aβ_{42} were believed to be disordered in the fibril state,[36,37,12] the mutation in the N-terminal has attracted a little attention of researchers. However, recent experiments[38−40] have suggested that residues at the N-terminal may be ordered and this terminal could carry some structural importance. The English (H6R),[41,42] Taiwanese (D7H),[43] and Tottori (D7N)[42,44,45] mutations alter the fibril formation rate and the survival of cells without affecting Aβ production.[42] The mutation A2V was found to enhance Aβ40 aggregation kinetics, but the mixture of the Aβ40 WT and A2V peptides protects against AD.[46] Using single-molecule atomic force microscopy (AFM) force spectroscopy, one can show that the N-terminal plays a key role in the peptide interaction in Aβ dimers.[47]

The all-atom replica exchange[48−51] molecular dynamics (REMD) simulations were performed to understand the influence of the mutation A2V on equilibrium ensemble of

Received: April 14, 2014
Revised: June 30, 2014

   dx.doi.org/10.1021/jp503652s | J. Phys. Chem. B XXXX, XXX, XXX−XXX

the truncated peptide $A\beta_{1-28}$.[52] The impact of D7N and H6R on the aggregation and structure dynamics of alloforms $A\beta_{40}$ and $A\beta_{42}$ has been studied in our previous simulations.[53,54] Contrary to D7N and H6R, D7H increased $A\beta$ production and $A\beta_{42}/\beta_{40}$ ratio. The effect of D7N on the fibril formation is two-fold: it elongates the lag phase but promotes the fibril formation in the sense that the oligomer and fibril expression is elevated as the ThT fluorescence intensity in the saturation phase is higher than that in WT.[43]

In this paper we present the structure changes of alloforms $A\beta_{40}$ and $A\beta_{42}$ peptides under Taiwanese D7H mutation using the REMD simulations with the OPLS force field[55,56] and implicit solvent[57] at the microsecond timescale. It is shown that, in accord with the experiments,[43] mutation D7H slows the fibril growth of both peptides $A\beta_{40}$ and $A\beta_{42}$. The mechanism underlying this effect is associated with the reduction of beta structures and enhanced flexibility of the salt bridge D23−K28. In addition, we predict that D7H has little impact on the collision cross section (CCS) of monomers of $A\beta$ peptides.

MATERIALS AND METHOD

Initial Structures of $A\beta$ Peptides and Their Mutants. The crystal structures of full-length $A\beta_{40}$ (PDB entry 1BA4[58]) and $A\beta_{42}$ (PDB entry 1Z0Q[59]), taken from the Protein Data Bank (PDB), are rich in helix as they have been solved in micellar solutions (Figure 1). The mutants $A\beta_{40}$-D7H and $A\beta_{42}$-D7H were obtained from the wild-type structures by using mutation tools in pymol.[60]

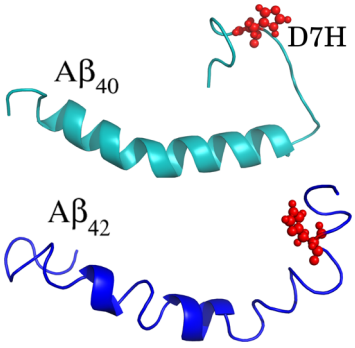

Figure 1. Initial structures for MD simulations of $A\beta_{40}$ and $A\beta_{42}$. Red refers to residue 7 where the mutation is made.

Terminology. The $A\beta$ peptide was segmented into 4 regions: the N-terminal (residues 1−16), the central hydrophobic core (CHC) (residues 17−21), the fibril-loop region (residues 22−29), and the C-terminal (residues 30−42). For simplicity in what follows, the WT and D7H monomers will be referred to as $A\beta_{40}$-WT, $A\beta_{40}$-D7H, $A\beta_{42}$-WT, and $A\beta_{42}$-D7H.

Molecular Dynamics Simulations. The GROMACS 4.5.5 package[61] was used to run molecular dynamics (MD) simulations with the OPLS-AA/L force field[56] and the implicit solvent using the generalized Born (GB) model.[62] The OPLS-AA force field was used because the OPLS-generated conformations for the $A\beta_{40}$ and $A\beta_{42}$ monomer match reasonably the NMR data.[63] In addition, many studies have shown that OPLS is suitable for exploring the aggregation of several $A\beta$ fragments[64] and gives results qualitatively similar to that found using the CHARMM force field for the $A\beta_{10-35}$ dimer.[65] The implicit solvent was chosen because of limitations of our computational facilities, but this would not affect much our main conclusion as we compare WT and mutant. The equations of motion were integrated by using a leapfrog algorithm[66] with a time step of 2 fs. The LINCS algorithm[67] was used to constrain the length of all bonds. The dielectric constant for the implicit solvent was set to 78.3. The V-rescale temperature coupling, which uses velocity rescaling with a stochastic term,[68] allows one to couple each system to a heat bath with a relaxation time of 0.1 ps. The van der Waals (vdW) forces were calculated with a cutoff of 1.4 nm, and the particle mesh Ewald method[69] was employed to treat the long-range electrostatic interactions. The nonbonded interaction pair list, with a cutoff of 1 nm, was updated every 10 fs.

For REMD simulation, the number of replicas is 12 for all systems. The temperature of replicas were determined by using the method recently proposed by Partrisson and van der Spoel[70,71] with requested acceptance ratio of ≈20%. The lowest and highest temperatures are 270 and 566 K for $A\beta_{40}$ systems and 270 and 566 K for $A\beta_{42}$ systems (T = 270.0, 290.2, 311.8, 334.5, 358.4, 383.5, 410.1, 438.0, 467.5, 498.5, 531.2, 566.0 K). Exchanges between replicas were attempted every 2 ps, which is large enough compared to the coupling time of the heat bath. Each replica was run for 1000 ns, and the data were collected every 10 ps.

Tools and Measures Used for Data Analysis. *Secondary Structure.* To estimate secondary structures of $A\beta_{1-40}$ peptide, we used the STRIDE algorithm[72,73] because the definition of secondary structures in this algorithm is based not only on dihedral angles but also on HBs.

Salt Bridge. A salt bridge (SB) between two charged residues was considered formed if the distance between two specific atoms remains within 4.6 Å. For SB 23−28, we consider the distance between C^{γ} atom of the Asp23 residue and the N^{ζ} atom of the residue Lys28.

Free-Energy Landscapes. The free-energy surface along the N-dimensional reaction coordinated $V = (V_1,...,V_N)$ is given by $\Delta G(V) = -k_B T[\ln P(V) - \ln P_{max}]$, where $P(V)$ is the probability distribution obtained from a histogram of MD data. P_{max} is the maximum of the distribution, which is subtracted to ensure that $\Delta G = 0$ for the lowest-free-energy minimum. We used dihedral principal component analysis (dPCA)[74] and the two most important eigenvalues V_1 and V_2 to construct the free-energy surface.

Collision Cross Section. The collision cross section of all dominant structures on the free-energy surface was also calculated using the MOBCAL software and the trajectory method,[75] which treats the molecule as a collection of atoms represented by a 12−6−4 potential and is often used for proteins.[76]

RESULTS AND DISCUSSION

Equilibration. To demonstrate the performance of the REMD algorithm, Figure S1 in Supporting Information shows the time evolution of exchange partners for $A\beta_{40}$-WT (similar results for other sequences are not shown). Clearly, during the course of the simulation each replica is visited many times by each trajectory; in other words, each trajectory performs a random walk in temperature space ensuring that our choice for the temperature set is reasonable. Furthermore, Figure S2 in Supporting Information shows the distribution of the potential energy for all of the replicas for $A\beta_{42}$-WT. As the temperature increases it becomes more and more broad. For adjacent temperatures the corresponding distributions have enough

dx.doi.org/10.1021/jp503652s | J. Phys. Chem. B XXXX, XXX, XXX−XXX

overlap, which guarantees reasonable exchange probabilities (≈ 20%).

To ascertain that our data are well-equilibrated, we calculated the secondary structure contents for two time windows $[t_{eq}, t_1]$ and $[t_{eq}, t_{full}]$. Here the equilibration time t_{eq} = 210 ns for all systems, while time of the entire MD run t_{full} = 800 and 1200 ns for $A\beta_{40}$ and $A\beta_{42}$ sequences, respectively. We chose t_1 approximately in the middle of t_{eq} and t_{full}, i.e., t_1 = 500 for $A\beta_{40}$ and 700 ns for $A\beta_{42}$. If the results obtained for two windows coincide, then the system can be considered to be equilibrated. For all four sequences, the β-contents obtained for two windows are essentially the same at T = 311.8 K (Figure 2)

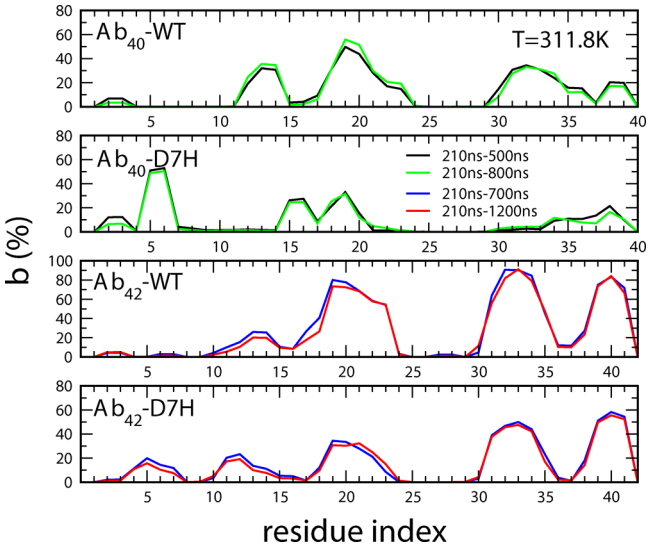

Figure 2. β-contents obtained for time windows [210, 500 ns] and [210, 800 ns] for $A\beta_{40}$ and [210, 700 ns] and [210, 1200 ns] for $A\beta_{42}$.

and T = 290.2 K (Figure S3 in Supporting Information), supporting convergence of our data. Similar results were also obtained for turn (Figures S4 and S5 in Supporting Information), helix, coil (not shown), and the distribution of end-to-end distance for four sequences (Figures S6 and S7 in Supporting Information). Thus, our replica exchange simulations provide the equilibrated data. Hereafter, results obtained for the wider time window will be presented.

Impact of D7N on Secondary Structures of $A\beta_{40}$. The mean value of β, helix, turn and coil contents, obtained in equilibrium at T = 311.8 K for $A\beta_{40}$-WT, is 12.7, 0.2, 62.1 and 25%, respectively (Table 1). Overall, our results with relatively poor beta structure (12.7%) and almost no helices (0.2%) agree with the experiments of Zhang et al.[77] and Danielsson et al.[78] showing that the Alzheimer's Aβ peptide adopts a collapsed coil structure in water.[77] Using filtration though 10 000 molecular weight cutoff, circular dichroism (CD) of all low molecular weight $A\beta_{40}$-WT aggregates gives 88% of random coil and turn, 12% of β-strand and 0% of α-helix at 295 K, pH 7.5 and day 0.[79] In contrast, another preparation of $A\beta_{40}$-WT aggregates gives a β-strand of 25% for the monomer.[80] Our 87% of coil + turn for $A\beta_{40}$-WT is in agreement with the first preparation (88%) and the discrete MD-MD multiscale approach (94%).[81]

Our simulations provide the α-content lower than that of previous coarse-grained UNRES[82] but comparable with that of all-atom results of Viet et al.[53,83] Sgourakis et al.[63] have used Amber-derived PARM94, PARM96, MOD-PARM, GROMOS, and OPLS force fields, while a recently improved version of the Amber force field PARM99SB has been employed by Yang and Teplow[84] to study dynamics of Aβ peptides in aqueous solution. Our estimate of β-content (12.8%) is compatible with the results reported by these groups. The REMD simulation protocol coupled with the OPLS-AA/L force field and the TIP3P water model yields $\beta \approx 25\%$, which seems to be high for $A\beta_{40}$.[85] The discrete molecular dynamics combined with the four-bead protein model gives $\beta \approx 19\%$ for full-length $A\beta_{40}$ and 15% for the truncated $A\beta_{3-40}$.[86] These estimations are a bit higher than ours.

Upon mutation, the total β-propensity of $A\beta_{40}$ is slightly reduced from 12.7 to 8.2% (Table 1), but the per-residue population varies along the sequence with the increase at residues 5 and 6 (Figure 3). The substantial reduction in the

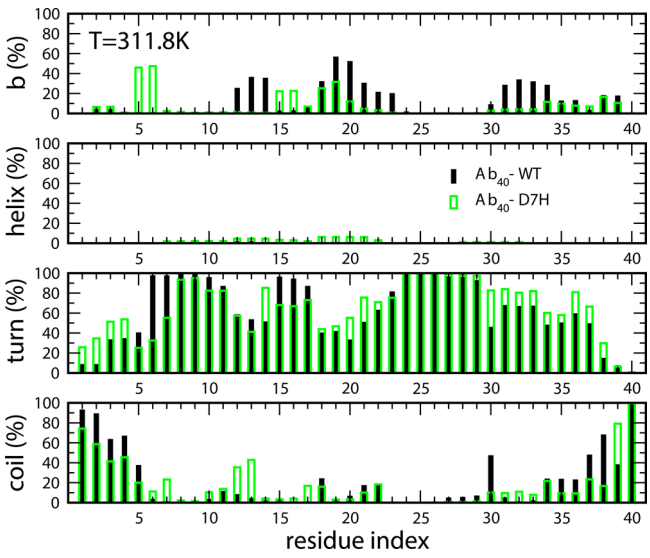

Figure 3. Distributions of secondary structure of $A\beta_{40}$ and its mutant at 311.8 K. Results were obtained from the time window [210, 800 ns] of MD simulations.

Table 1. Average Secondary Structures of $A\beta_{40}$ and $A\beta_{42}$ and Its Mutant (D7H)[a]

	$A\beta_{40}$		$A\beta_{42}$	
content (%)	WT	D7H	WT	D7H
β	12.7 ± 3.2	8.2 ± 3.0	26.2 ± 3.6	14.4 ± 4.2
α	0.2 ± 1.3	1.6 ± 2.5	0.0 ± 0.0	1.0 ± 2.4
turn	62.1 ± 4.9	65.4 ± 4.8	52.6 ± 4.2	62.7 ± 5.0
coil	25.0 ± 3.1	24.8 ± 4.5	21.2 ± 3.2	21.9 ± 4.1

[a]The data is the average of the last 800 ns for $A\beta_{40}$ systems and 1200 ns for $A\beta_{42}$ systems at 311.8 K.

regions 12−23 and 30−39 while leaving the turn in the loop region 22−29 almost unchanged implies that, in accord with experiment, the mutation retards the fibril formation because the population of the fibril-prone state **N*** is decreased.[65,87] As follows from Table 1 and Figure 3, the mutation has a minor effect not only on the overall content of α-helix, turn, and coil but also on their per-residue propensities.

One can show that the influence of D7H on the secondary structures at 290.2 K is similar to that at T = 311.8 K (Figure S8 and Table S1 in Supporting Information). Thus, the depression of aggregation is also expected at this temperature.

dx.doi.org/10.1021/jp503652s | J. Phys. Chem. B XXXX, XXX, XXX−XXX

Impact of D7N on Secondary Structures of Aβ_{42}. We first compare our results obtained by the OPLS force field with implicit solvent for Aβ_{42}-WT with those of the previous studies. As follows from Figures 3 and 4 and Table 1, the β-strand

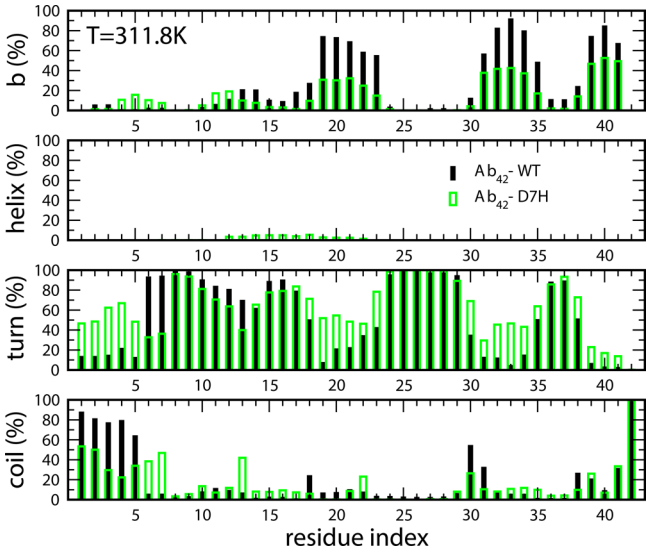

Figure 4. Distributions of secondary structure of Aβ_{42} and its mutant at 311.8 K. Results were obtained from the time window [210, 1200 ns] of MD simulations.

abundance of Aβ_{42}-WT (26.2%) is markedly higher than that of Aβ_{40}-WT (12.7%). This is consistent with the results reported in prior theoretical works[26,53,63,84,88,89] and the experimental observation[90] that Aβ_{42} aggregates much faster than Aβ_{40}, having higher population of fibril-prone state **N***.[87] The high β-content occurs at residues 19−23 (Figure 4), which is consistent with Rosenman et al.[85] who observed high β-population at residues 16−23 using the OPLS-AA/L force field with explicit water model TIP3P. Having performed all-atom simulations with Amber ff99SB force field and TIP4P-Ew water, one can show that region 16−21 is rich in β-structure.[91]

The C-terminal is rich in β-propensity (Figure 4) at residues 31−35 and 39−41, whereas other theoretical studies showed that the β-structure is mainly located in region 38−41,[63] 32−36,[84] 27−37,[85] 29−36,[91] or 37−40.[83] The C-terminal is much more ordered than the N-terminal, and this is in line with the fact that the C-terminal is fibril-prone, as observed in the experiment of Luhrs et al.[12] and with the simulations in which the Aβ_{42} fibril growth initiates from this terminal.[92] Contrary to our other theoretical studies, it was shown that the C-terminal is poorer in β-structure than the N-terminal[25] using the implicit solvent coarse-grained model OPEP. It remains unclear if this is due to drawbacks of coarse-graining or other reasons. The discrete MD coupled with the four-bead model has also predicted a β-strand in the N-terminus.[88] The β-content obtained in our simulations is higher than that of Velez-Vega and Escobedo,[93] Yang and Teplow,[84] and Cote et al.[25] but significantly lower than the result reported by Mitternacht et al.[29] Such an abundance of β-structure, obtained by these authors, may be associated with omission of the electrostatic interaction in their force field.[94]

As in the Aβ_{40} case, the α-content of Aβ_{42}-WT is almost zero (Table 1). This is comparable with results of other groups,[25,93,95] but lower than that reported by Yang and Teplow.[84] In equilibrium, the random coil (coil + turn) is 72.4% (Table 1), implying that Aβ_{42} is more structured than Aβ_{40} having random coil of 87%. Our result falls into the range of other theoretical estimates,[25,63,84,93] but is lower than that of Mitternacht et al.[29]

Upon mutation, the β-content drops from 26.2% to 14.4% (Table 1). Because the substantial reduction occurs at fibril-prone regions expanded over residues 19−23, 31−35, and 39−41, one can expect that, in accord with experiment,[43] D7H slows aggregation. The mutation levels up the turn from 52.6% to 62.7% (Table 1), and the increase of turn at segments 19−21 and 30−41 (Figure 4) provides further support for the experimental finding. The enhancement of the turn content at residues 22−23 in the fibril-loop region probably has minor impact on the fibril formation. The overall propensity of α-helix and coil remains almost untouched by the mutation, but we see variations of per-residue distributions of coil along the sequence (Figure 4). The impact of coil enhancement at residues 6, 7, and 13 in the disordered fragment is presumably canceled out by its decrease at positions 1−5 from the same fragment.

The effect of mutation at T = 290.2 K is similar to that at T = 311.8 K, as is evident in Table S1 and Figure S9 in Supporting Information. Therefore, D7H is expected to slow the fibril formation at this temperature.

Mutation Slightly Alters the Collision Cross Section. *Free-Energy Surfaces.* The free-energy surfaces (FESs) and the dominant structures of four species, obtained in the equilibrium at 311.8 K, are shown in Figure 5. The FES of Aβ_{40}-D7H is broader along V_2 and a bit more complex than WT, but both of them have four dominant basins. Table 2 gives for each free-energy local minima its population, the secondary structure composition, and the CCS. In Aβ_{40}-WT structures, S2 and S4 are more ordered than S1 and S3 as their β-content $\beta \approx 30$ and 15%. In terms of β-content, S2 and S4 are compatible with the most dominant structures obtained by Ball et al.[91] and Rosenman et al.[85] The α-content of all representative structures is zero, while the coil varies between 10% of S2 and 37% of S3, and the turn is in the range of 60−78%. Two short β-strands with β = 15% occur in S1 of Aβ_{40}-D7H, whereas S2 and S3 contain α-helix. The low populated S4 has neither β- nor α-structure, and its coil (70%) is poorer than its turn (30%). Overall, the dominant structures in Figure 5 correctly describe the main impact of mutation that reduces the β-structure.

Similar to the Aβ_{40} case, the mutation makes the FES of Aβ_{42} broader but in both axes V_1 and V_2 (Figure 5). Except structure S3, which has population of only 19%, the dominant structures of Aβ_{42}-WT contain β-strands, and this is consistent with the result of Ball et al.[91] showing that β-strands occur in all representative conformations. However, Rosenman et al. reported that[85] only the most important structure with population of 46% has two β-strands.

The sharp difference between WT and D7H is that the two most populated structures of WT contain β-strands, which it is not the case for D7H (Table 2). A total population of S1, S2, S4, and S5 of Aβ_{42}-WT that have β-structures is 81% versus 64% of S3 and S4 on the Aβ_{42}-D7H FES. The first two minima, representing 54% and 51% of all conformations for the WT and D7H sequences, respectively, have the mean coil 19% and ≈40% in WT and D7H species, resprectively. Their turn in WT is also lower than in D7H.

Collision Cross Section. Using dehydrated and energy-minimized dominant structures on the FES (Figure 5) and the trajectory method,[75] we have computed CCSs for all sequences (Table 2). The mean value of CCS of Aβ_{40}-WT is equal 717 ±

dx.doi.org/10.1021/jp503652s | J. Phys. Chem. B XXXX, XXX, XXX−XXX

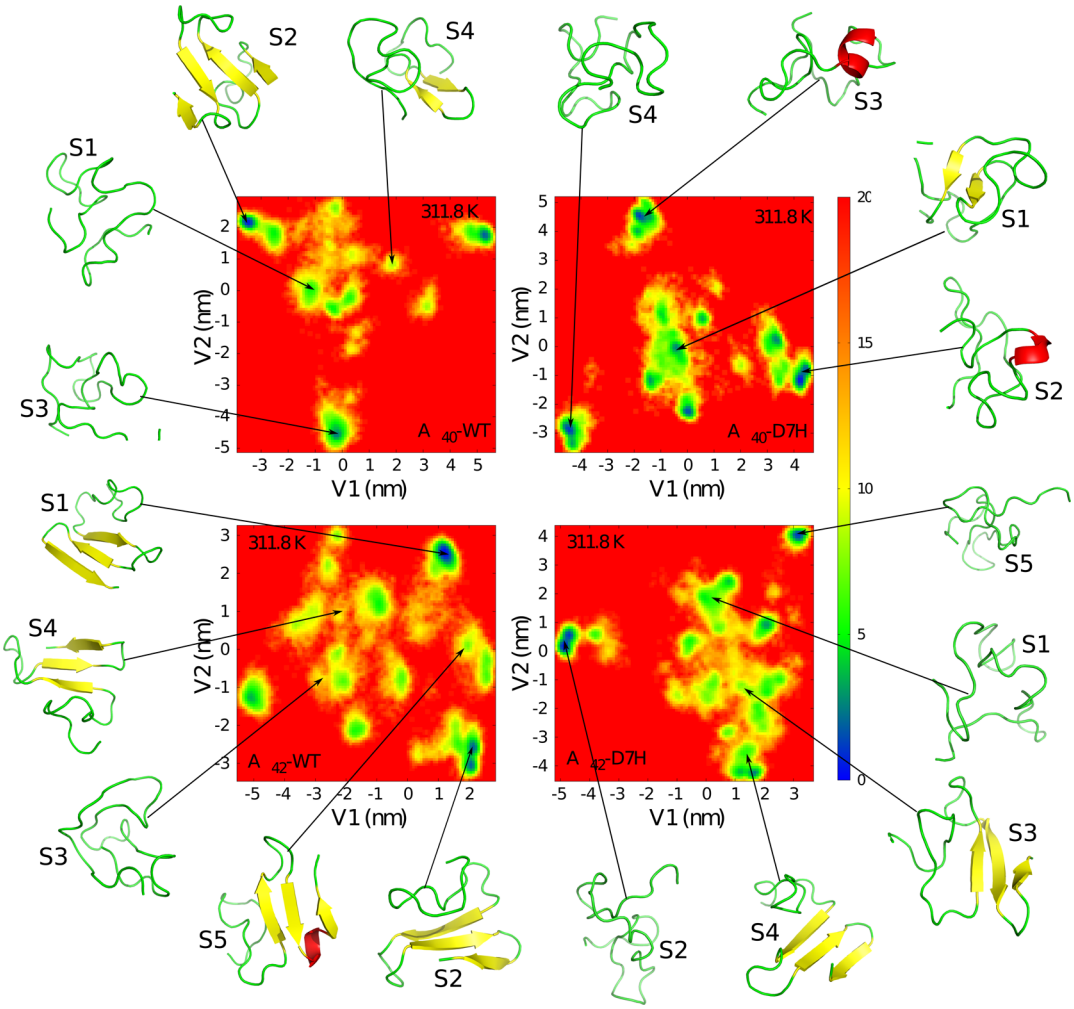

Figure 5. Free-energy landscape of Aβ_{40} and Aβ_{42} and their mutants as a function of the first two principal components V1 and V2. The results were obtained from the dPCA analysis at 311.8 K.

16 Å^2 at 311.8 K. The mutation slightly changes this result to 694 ± 21 Å^2 for Aβ_{40}-D7H. We obtained CCS of 756 ± 21 Å^2 and 749 ± 18 Å^2 for β_{42}-WT and Aβ_{42}-D7N, respectively. The ion-mobility-based mass spectroscopy experiment[96,97] gives CSSs equal 679 ± 8 for Aβ_{40} and 693 ± 8 Å^2 for Aβ_{42}. Thus, our results fall in the range of experimental estimations, but the best agreement with the experiment was obtained for structure S1 of Aβ_{40}-WT with CCS of 689 Å^2 (Table 2). Using the REMD with a generalized Born approximation, Baumketner et al. also determined a CCS of 765 Å^2 for Aβ_{42}-WT, which is very close to our estimation of 756 ± 21 Å^2. Utilizing the conventional MD with OPLS force field and explicit water, Viet et al.[53] have obtained 750 ± 13 Å^2 and 783 ± 48 Å^2 for Aβ_{40}-WT and Aβ_{42}-WT, respectively. Within the error bars these estimations are comparable with ours. Gessel et al. reported that the CCS does not vary much upon mutation D7N, A21G, and E22G.[96] Our finding is in qualitative agreement with this finding that D7H also has little effect on CCSs (Table 2).

We have constructed the FES for all sequences at T = 290.2 K (Figure S10 in Supporting Information). The structural characteristics and SSC of dominant structures are given in Table S2. The mean values of SSC are 712 ± 20, 693 ± 10, 727 ± 23, and 724 ± 11 Å^2 for Aβ_{40}-WT, Aβ_{40}-D7H, Aβ_{42}-WT, and Aβ_{42}-D7H, respectively. Within the error bars, the estimations for WT are in the range of the experimental data.[96,97] At the lower temperature, the structure of peptides becomes more compact, manifesting in narrower CCS compared to that at T = 311.8 K.

Impact of D7H on the Bending Free Energy and Fibril Formation Rates. Figures S11 and S12 in Supporting Information show the distributions of the distance between C$^\gamma$ atom of the Asp23 residue and the N$^\zeta$ atom of the residue Lys28 at 311.8 K and 290.2 K, respectively. Assuming that SB is formed if the distance between C^γ_{23} and N^ζ_{28} is smaller than 4.6 Å, then the lifetimes of WT as well as mutants are very short. For Aβ_{42}, the SB becomes more flexible upon mutation, suggesting that D7H retards the fibril formation observed in the experiments. This effect is much less visible from the SB dynamics of Aβ_{40} sequences.

Assuming that the mechanism of acceleration of fibril formation by mutation is governed by the constraint of the salt bridge 23−28 as suggested by other computational studies[65] and by the role of a lactam bridge connecting residues 23−28 that suppresses the lag phase prior to Aβ_{40} nucleation,[98] we can estimate the bending free energy as follows:

$$\Delta G_{\text{bend}} = -k_B T \ln \frac{P(R^\alpha_{23-28} < \bar{R}^\alpha_{23-28})}{P(R^\alpha_{23-28} > \bar{R}^\alpha_{23-28})} \quad (1)$$

dx.doi.org/10.1021/jp503652s | J. Phys. Chem. B XXXX, XXX, XXX−XXX

Table 2. Characterization of the Conformational States (S) of the WT and D7H $A\beta_{40}$ and $A\beta_{42}$ Indicated on the Free-Energy Landscapes[a]

system	S	P	β	α	turn	coil	CCS
$A\beta_{40}$-WT	1	29	0	0	78	22	689
	2	28	30	0	60	10	729
	3	23	0	0	63	37	726
	4	20	15	0	63	22	724
$A\beta_{40}$-D7H	1	39	15	0	65	20	682
	2	29	0	8	60	32	692
	3	17	0	13	77	10	703
	4	15	0	0	70	30	689
$A\beta_{42}$-WT	1	29	29	0	52	19	766
	2	25	31	0	50	19	725
	3	19	0	0	60	40	725
	4	17	21	0	48	31	797
	5	10	30	7	69	3	768
$A\beta_{42}$-D7H	1	27	0	0	62	38	744
	2	24	0	0	57	43	740
	3	21	33	0	55	12	761
	4	17	31	0	55	14	761
	5	11	0	0	71	29	738

[a]Shown are the population P (percent), the secondary structure contents (percent), and collision cross section (square angstroms) at T = 311.8.2 K.

where $\bar{R}^{\alpha}_{23-28}$ is an average Cα distance between residues 23 and 28 and $P(R^{\alpha}_{23-28} < \bar{R}^{\alpha}_{23-28})$ and $P(R^{\alpha}_{23-28} > \bar{R}^{\alpha}_{23-28})$ are the probabilities of having the SB distance smaller and greater than $\bar{R}^{\alpha}_{23-28}$, respectively. The distributions of Cα distances for four sequences are shown in Figure 6 for T = 311.8 K and Figure S9 for T = 290.2 K; $P(R^{\alpha}_{23-28} < \bar{R}^{\alpha}_{23-28})$ and $P(R^{\alpha}_{23-28} > \bar{R}^{\alpha}_{23-28})$ are given in Table 3 and Table S3 in Supporting Information.

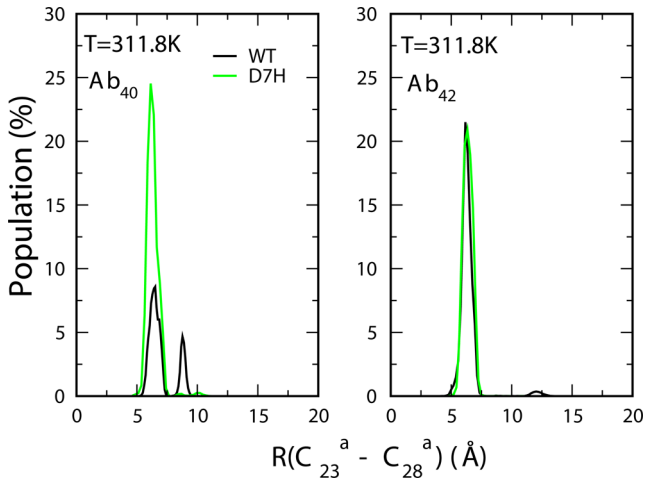

Figure 6. Distributions of Cα distances of salt bridges of $A\beta_{40}$ and $A\beta_{42}$ sequences at 311.8 K. Black and green lines refer to WT and D7H, respectively.

The mutation shifts the bending free energy by $\Delta\Delta G_{bend} = \Delta G_{bend}(D7H) - \Delta G_{bend}(WT)$. At T = 290.2 K, using data in Table S3 in Supporting Information, we obtain $\Delta\Delta G_{bend}/k_BT = -0.494 \pm 0.08$ and -0.544 ± 0.07 for $A\beta_{40}$ and $A\beta_{42}$, respectively. Because $\Delta\Delta G_{bend}$ is related to the fibril formation rates κ_{WT} and κ_{D7H} as $\Delta\Delta G_{bend} = k_BT \ln(\kappa_{D7H}/\kappa_{WT})$, the mutation slows fibril formation by 0.61 and 0.58 times for $A\beta_{40}$ and $A\beta_{42}$, respectively. Using data in Table 3 one can show that for T = 311.8 K the aggregation rates are reduced by 0.59 and 0.64 times for $A\beta_{40}$ and $A\beta_{42}$, respectively (Table 4). Thus, our results are in good agreement with experiments[43] which point to about 2-fold rate decrease for both peptides. It should be noted that the effect of the Taiwan mutation is in sharp contrast with that of the Tottori mutant D7N which leads to nearly 10-fold enhancement in fibril growth.[45]

Table 3. Distribution of CA22−CA28 and CA23−CA28 Distances (Angstroms) of $A\beta_{40}$ and $A\beta_{42}$ and its Mutant Systems at 311.8 K

peptide	$A\beta_{40}$-WT	$A\beta_{40}$-D7H	$A\beta_{42}$-WT	$A\beta_{42}$-D7H
$\bar{R}_{23-28}$ (Å)	7.01	6.46	6.49	6.49
$P(R > \bar{R}_{23-28})$ (%)	30.05	42.15	37.56	48.59
$P(R < \bar{R}_{23-28})$ (%)	69.95	57.85	62.44	51.41

Table 4. Reduction of Fibril Formation Rates by Mutation D7H for $A\beta_{40}$ and $A\beta_{42}$

	reduction of aggregation rates	
peptide	$A\beta_{40}$	$A\beta_{42}$
311.8 K	0.59	0.64
290.2 K	0.61	0.58

Comparison between Mutants D7N and D7H. A turn at Ser8-Gly9 might be particularly important because it can bring the N-terminal quarter of the peptide into contact with the CHC region modulating substantially the $A\beta$ assembly kinetics.[99] Being in proximity with the putative Ser8-Gly9 turn the mutations D7H and D7N may affect it and through this effect alter the aggregation rate.[45] This point of view is supported by simulations on all D7N species with an increased turn propensity at residues 5−12 ($A\beta_{40}$ monomer) and 1−9 ($A\beta_{42}$ monomer).[53] Upon D7H mutation, the turn content at Ser8-Gly9 remains unchanged in $A\beta_{40}$ and $A\beta_{42}$ monomers (Figures 3 and 4). It increases at residues 1−4 for $A\beta_{40}$ and at 1−5 for $A\beta_{42}$, but reduction occurs at 5−7 for $A\beta_{40}$ and 6−7 for $A\beta_{42}$. Thus, the effect of D7H on the proximity of the N-terminal quarter with the CHC region is less pronounced than that of D7N. This agrees with the experimental observations that D7N accelerates the lag phase by ≈10-fold in $A\beta_{40}$ and ≈5-fold in $A\beta_{42}$ system,[45] while the slowing by D7H is only 2-fold.[43]

The experimental study of temporal changes in the secondary structure[45] revealed that D7N accelerates the conversion from random coil to β-sheet via α-helix. This observation was supported by our previous simulations[53] that D7N reduces coil by 5% and 14% in $A\beta_{40}$ and $A\beta_{42}$. If we consider turn and coil as random coil, then upon mutation D7H, the random coil levels up ≈2% in $A\beta_{40}$ and 12% in $A\beta_{42}$, supporting the aggregation retardation.[43]

Upon D7N mutation, the overall charge at the N-terminal is reduced resulting in a weaker repulsion between two chains and consequently in faster aggregation. The D7H mutation also reduces the net charge of $A\beta$ peptides, but at neutral pH, histidine as a basic polar can be either neutral (90%) or positively charged (10%), leading to less impact on the assembly kinetics compared to D7N. This is in qualitative agreement with the experiments and our simulations.

Reliability of Results Obtained in Implicit Solvent. The reliability of our implicit solvent results may be checked by

dx.doi.org/10.1021/jp503652s | J. Phys. Chem. B XXXX, XXX, XXX−XXX

examining stability of the dominant states on FES (Figure 5) in explicit solvent. We have carried out 40 ns simulations using the OPLS-AA/L force field and TIP4P water model,[100] and dominant structures S1, S2, S3, and S4 are shown in Figure 5 as initial configurations for four sequences. Note that TIP4P is the most suitable for this force field.[101,102] The peptides were solvated in octahedrons of 5.3 nm size with about 3600 water molecules. Figure S14 in Supporting Information shows the time evolution of the Cα RMSD of structures S1−S4 of Aβ_{42}-D7H from their implicit solvent structures. Because the mean value of RMSD is lower than 0.45 nm, these structures remain stable in the explicit solvent. This conclusion is valid not only for Aβ_{42}-D7H but also for other sequences (results not shown). The additional information about the stability of implicit solvent basins may be gained also from variation of secondary structures during the simulation course. Figure S15 in Supporting Information shows the time dependence of secondary structures obtained in the explicit solvent for Aβ_{42}-D7H (similar results for the remaining sequences are not shown). Because these quantities fluctuate around their equilibrium value, the implicit basins are stable against the explicit solvent. This conclusion is also supported by data shown in Table S4 in Supporting Information, in which the mean secondary structures obtained in both aqueous models are essentially the same.

CONCLUSION

We have studied the influence of the D7H mutation on structure changes of Aβ monomers using long all-atom MD simulations in implicit water and different tools for data analysis. Through sampling in the microsecond timescale we are in a position to understand some experimental results at least at the qualitative level.

Our data support the experimental finding that D7H retards fibril growth through the same mechanism for Aβ_{40} and Aβ_{42}. Namely, for both species the reduction of the overall β-structure and at the fibril-prone regions is responsible for the slowing down of association. Although the estimation of relative fibril formation rates based on the bending free energy of SB 23−28 is approximate, it provides complementary insight into the effect of mutations. The 2-fold reduction in fibril formation rates predicted by this approach is in reasonable accord with the experiment. Once the multiscale simulations were performed, it was demonstrated that basins obtained in implicit solvent remain stable in explicit solvent. This suggests that our results are also valid for explicit aqueous models.

We have shown that the Taiwan familial disease mutation has little impact on the CCS of alloform Aβ peptides, implying that this parameter is not sensitive enough to probe structural changes. Although the CCS of D7H was not experimentally measured, our result is in the qualitative agreement with the experiments showing that other mutations like D7N, A21G, and E22G have no noticeable effect on the CCS of both monomers and oligomers.

For the first time our study provides a detailed atomistic picture of conformational changes of A$\beta_{40/42}$ monomers upon the Taiwanese mutation. Our results are useful for understanding experimental findings on self-assembly kinetics and the collision cross-section.

Finally, computational studies of structural dynamics of Aβ dimers provide useful insights on differences of Aβ_{40} and Aβ_{42} as well as on mechanisms of aggregation.[103−105] Therefore, it would be interesting to consider the impact of the Taiwan familial disease mutation on oligomerization of Aβ peptides. Our work in this direction is in progress.

ASSOCIATED CONTENT

Supporting Information

Secondary structures of four sequences at T = 290.2 K (Table S1); main characteristics of dominant structures at T = 290.2 K (Table S2); distribution of $C^{\alpha}_{23}-C^{\alpha}_{28}$ distance at T = 290.2 K (Table S3); dominant structures obtained in the implicit and explicit solvent (Table S4); random walk of the first and last replicas in temperature space during simulation course (Figure S1); distributions of the potential energy of Aβ_{42}-WT for all of the replicas (Figure S2); secondary structures and the distributions of the end-to-end distance obtained in short and full time windows (Figure S3−S7); per-residue distributions of secondary structures at T = 290.2 K (Figures S8 and S9); free-energy surface at T = 290.2 K (Figure S10); distributions of the 23−28 salt bridge distance (Figures S11−S13); time dependence of RMSD and secondary structures obtained in explicit solvent (Figures S14 and S15). This material is available free of charge via the Internet at http://pubs.acs.org.

AUTHOR INFORMATION

Corresponding Author

*E-mail: masli@ifpan.edu.pl. Phone: +48 22 843 66 01.

Author Contributions

$^{\perp}$P.M.T. and M.H.V. contributed equally to this work

Notes

The authors declare no competing financial interest.

ACKNOWLEDGMENTS

We thank Vuong Van Quan and Y-R. Chen for very useful discussions. The work was supported by Narodowe Centrum Nauki in Poland (Grant 2011/01/B/NZ1/01622), Vietnam National Foundation for Science and Technology Development (NAFOSTED) under grant number 106-YS.02-2013.01, Department of Science and Technology at Ho Chi Minh city, and Grants NSC 102-2112-M-0011-006 and NCTS from Taiwan. Allocation of CPU time at the supercomputer center TASK in Gdansk (Poland) is highly appreciated.

REFERENCES

(1) Henderson, A. S.; Jorm, A. F. *Dementia*; John Wiley & Sons Ltd: New York, 2002; Chapter 1.

(2) Greene, J. D. W.; Baddeley, A. D.; Hodges, J. R. Analysis of the Episodic Memory Deficit in Early Alzheimers Disease: Evidence from the Doors and People Test. *Neuropsychologia* **1996**, *34*, 537−551.

(3) Price, B. H.; Gurvit, H.; Weintraub, S.; Geula, C.; Leimkuhler, E.; Mesulam, M. Neuropsychological Patterns and Language Deficits in 20 Consecutive Cases of Autopsy-confirmed Alzheimer's Disease. *Arch. Neurol. (Chicago)* **1993**, *50*, 931−937.

(4) Esteban-Santillan, C.; Praditsuwan, R.; Ueda, H.; Geldmacher, D. S. Clock Drawing Test in very Mild Alzheimer's Disease. *J. Am. Geriatr. Soc.* **1998**, *46*, 1266−1269.

(5) Hardy, J.; Selkoe, D. J. Medicine - The Amyloid Hypothesis of Alzheimer's Disease: Progress and Problems on the Road to Therapeutics. *Science* **2002**, *297*, 353−356.

(6) Alonso, A.; Zaidi, T.; Novak, M.; Grundke-Iqbal, I.; Iqbal, K. Hyperphosphorylation Induces Self-assembly of Tau into Tangles of Paired Helical Filaments/Straight Filaments. *Proc. Natl. Acad. Sci. U.S.A.* **2001**, *98*, 6923−6928.

(7) Citron, M. Strategies for Disease Modification in Alzheimer's Disease. *Nat. Rev. Neurosci.* **2004**, *5*, 677−685.

(8) Aguzzi, A.; O'Connor, T. Protein Aggregation Diseases: Pathogenicity and Therapeutic Perspectives. *Nat. Rev. Drug Discovery* **2010**, *9*, 237−248.
(9) Eanes, E. D.; Glenner, G. G. X-ray Diffraction Studies on Amyloid Filaments. *J. Histochem. Cytochem.* **1968**, *16*, 673−677.
(10) Kirschner, D. A.; Abraham, C.; Selkoe, D. J. X-ray-diffraction from Intraneuronal Paired Helical Filaments and Extraneuronal Amyloid Fibers in Alzheimers-disease Indicates Cross-beta Conformation. *Proc. Natl. Acad. Sci. U.S.A.* **1986**, *83*, 503−507.
(11) Petkova, A. T.; Ishii, Y.; Balbach, J.; Antzutkin, O.; Leapman, R.; Delaglio, F.; Tycko, R. A Structural Model for Alzheimer's β-amyloid Fibrils based on Experimental Constraints from Solid State NMR. *Proc. Natl. Acad. Sci. U.S.A.* **2002**, *99*, 16742−16747.
(12) Luhrs, T.; Ritter, C.; Adrian, M.; Riek-Loher, D.; Bohrmann, B.; Doeli, H.; Schubert, D.; Riek, R. 3D Structure of Alzheimer's Amyloid-β(1−42) Fibrils. *Proc. Natl. Acad. Sci. U.S.A.* **2005**, *102*, 17342−17347.
(13) Kayed, R.; Head, E.; Thompson, J. L.; McIntire, T. M.; Milton, S. C.; Cotman, C. W.; Glabe, C. G. Common Structure of Soluble Amyloid Oligomers Implies Common Mechanism of Pathogenesis. *Science* **2003**, *300*, 486−489.
(14) Caughey, B.; Lansbury, P. T. Protofibrils, Pores, Fibrils, and Neurodegeneration: Separating the Responsible Protein Aggregates from the Innocent Bystanders. *Annu. Rev. Neurosci.* **2003**, *26*, 267−298.
(15) Walsh, D. M.; Selkoe, D. J. Aβ Oligomers — A Decade of Discovery. *J. Neurochem.* **2007**, *101*, 1172−1184.
(16) Lue, L. F.; Kou, Y. M.; Roher, A. E. Soluble Amyloid β Peptide Concentration as a Predictor of Synaptic Change in Alzheimer's Disease. *Am. J. Pathol.* **1999**, *155*, 853−862.
(17) Querfurth, H. W.; Laferla, F. M. Mechanisms of Disease Alzheimer's Disease. *N. Engl. J. Med.* **2010**, *362*, 329−344.
(18) Hendriks, L.; van Duijin, C. M.; Cras, P.; Cruts, M.; Hul, W. V.; van Harskamp, F.; Warren, A.; McInnis, M. G.; Antoarakis, S. E.; Martin, J.-J.; Hofman, A.; Broekhoven, C. V. Presenil Dementia and Cerebral Haemorrhage Linked to a Mutation at Codon 692 of the β-amyloid Precursor Protein Gene. *Nat. Genet.* **1992**, *1*, 218−221.
(19) Levy, E.; Carman, M. D.; Fernandez-Madrid, I. J.; Power, M. D.; Lieberburg, I.; van Duinen, S. G.; Bots, G. T. A. M.; Luyendijk, W.; Frangione, B. Mutation of the Alzheimer's Disease Amyloid Gene in Hereditary Cerebral Hemorrhage, Dutch Type. *Science* **1990**, *1*, 1124−1126.
(20) Bugiani, O.; Padovani, A.; Magoni, M.; Andora, G.; Sgarzi, M.; Savoiardo, M.; Bizzi, A.; Giaccone, G.; Rossi, G.; Tagliavini, F. An Italian type of HCHWA. *Neurobiol. Aging* **1998**, *19*, S238.
(21) Kamino, K.; Orr, H. T.; Payami, H.; Wijman, E. M.; Pulst, S. M.; Anderson, L.; O'dahl, S.; Nemens, E.; White, J. A.; et al. Linkage and Mutational Analysis of Familial Alzheimer Disease Kindreds for the APP Gene Region. *Am. J. Hum. Genet.* **1992**, *51*, 998−1014.
(22) Grabowski, T. J.; Cho, H. S.; Vonsattel, J. P.; Rebeck, G. W.; Greenberg, S. M. Novel Amyloid Precursor Protein Mutation in an Iowa Family with Dementia and Severe Cerebral Amyloid Angiopathy. *Ann. Neurol.* **2001**, *49*, 697−705.
(23) Tomiyama, T.; Nagata, T.; Shimada, H.; Teraoka, R.; Fukushima, A.; Kanemitsu, H.; Takuma, H.; Kuwano, R.; Imagawa, M.; Ataka, S.; et al. A New Amyloid β Variant Favoring Oligomerization in Alzheimer's-type Dementia. *Ann. Neurol.* **2008**, *63*, 377−387.
(24) Massi, F.; Straub, J. E. Probing the Origins of Increased Activity of the E22Q "Dutch" Mutant Alzheimer's β-amyloid Peptide. *Biophys. J.* **2001**, *81*, 697−709.
(25) Cote, S.; Derreumaux, P.; Mousseau, N. Distinct Morphologies for Amyloid Beta Protein Monomer: Aβ_{1-40}, Aβ_{1-42}, and Aβ_{1-40}(D23N). *J. Chem. Theor. Comp.* **2011**, *7*, 2584−2592.
(26) Lin, Y.-S.; Pande, V. S. Effects of Familial Mutations on the Monomer Structure of Aβ_{42}. *Biophys. J.* **2012**, *103*, L47−L49.
(27) Huet, A.; Derreumaux, P. Impact of the Mutation A21G (Flemish Variant) on Alzheimer's β-amyloid Dimers by Molecular Dynamics Simulations. *Biophys. J.* **2006**, *91*, 3829−3840.
(28) Coskuner, O.; Wise-Scira, O.; Perry, G.; Kitahara, T. The Structures of the E22Δ Mutant-type Amyloid-β Alloforms and the Impact of E22Δ Mutation on the Structures of the Wild-type Amyloid-β Alloforms. *ACS Chem. Neurosci.* **2013**, *4*, 310−320.
(29) Mitternacht, S.; Staneva, I.; Hard, T.; Irback, A. Comparing the Folding Free-energy Landscapes of Aβ42 Variants with Different Aggregation Properties. *Proteins* **2010**, *78*, 2600−2608.
(30) Krone, M. G.; Baumketner, A.; Bernstein, S. L.; Wyttenbach, T.; Lazo, N. D.; Teplow, D. B.; Bowers, M. T.; Shea, J. E. Effects of Familial Alzheimer's Disease Mutations on the Folding Nucleation of the Amyloid β-protein. *J. Mol. Biol.* **2008**, *381*, 221−228.
(31) Baumketner, A.; Krone, M. G.; Shea, J.-E. Role of the Familial Dutch Mutation E22Q in the Folding and Aggregation of the 15−28 Fragment of the Alzheimer Amyloid-β Protein. *Proc. Natl. Acad. Sci. U.S.A.* **2008**, *105*, 6027−6032.
(32) Hung, L. W.; Ciccotosto, G. D.; Giannakis, E.; Tew, D. J.; Perez, K.; Masters, C. L.; Cappai, R.; Wade, J. D.; Barnham, K. J. Amyloid-β Peptide (Aβ) Neurotoxicity is Modulated by the Rate of Peptide Aggregation: Aβ Dimers and Trimers Correlate with Neurotoxicity. *J. Neurosci.* **2008**, *28*, 11950−11958.
(33) Harmeier, A.; Wozny, C.; Rost, B. R.; Munter, L. M.; Hua, H. Q.; Georgiev, O.; Beyermann, M.; Hildebrand, P. W.; Weise, C.; Schaffner, W.; Schmitz, D.; Multhaup, G. Role of Amyloid-β Glycine 33 in Oligomerization, Toxicity, and Neuronal Plasticity. *J. Neurosci.* **2009**, *29*, 7582−7590.
(34) Munter, L. M.; Voigt, P.; Harmeier, A.; Kaden, D.; Gottschalk, K. E.; Weise, C.; Pipkorn, R.; Schaefer, M.; Langosch, D.; Multhaup, G. GxxxG Motifs within the Amyloid Precursor Protein Transmembrane Sequence are Critical for the Etiology of Aβ42. *EMBO J.* **2007**, *26*, 1702−1712.
(35) Lu, Y.; Wei, G. H.; Derreumaux, P. Effects of G33A and G33I Mutations on the Structures of Monomer and Dimer of the Amyloid-β Fragment 29−42 by Replica Exchange Molecular Dynamics Simulations. *J. Phys. Chem. B* **2011**, *115*, 1282−1288.
(36) Petkova, A. T.; Yau, W. M.; Tycko, R. Experimental Constraints on Quaternary Structure in Alzheimer's β-Amyloid Fibrils. *Biochemistry* **2006**, *45*, 498−512.
(37) Paravastu, A. K.; Leapman, R. D.; Yau, W. M.; Tycko, R. Molecular Structural Basis for Polymorphism in Alzheimer's β-amyloid Fibrils. *Proc. Natl. Acad. Sci. U.S.A.* **2008**, *105*, 18349−18354.
(38) Bertini, I.; Gonnelli, L.; Luchinat, C.; Mao, J. F.; Nesi, A. A New Structural Model of Aβ_{40} Fibrils. *J. Am. Chem. Soc.* **2011**, *133*, 16013−16022.
(39) Scheidt, H. A.; Morgado, I.; Rothemund, S.; Huster, D. Dynamics of Amyloid β Fibrils Revealed by Solid-state NMR. *J. Biol. Chem.* **2012**, *287*, 2017−2021.
(40) Lu, J. X.; Qiang, W.; Yau, W. M.; Schwieters, C. D.; Meredith, S. C.; Tycko, R. Molecular Structure of β-amyloid Fibrils in Alzheimer's Disease Brain Tissue. *Cell* **2013**, *154*, 1257−1268.
(41) Janssen, J. C.; Beck, J. A.; Campbell, T. A.; Dickinson, A.; Fox, N. C.; Harvey, R. J.; Houlden, H.; Rossor, M. N.; Collinge, J. Early Onset Familial Alzheimer's Disease: Mutation Frequency in 31 Families. *Neurology* **2003**, *60*, 235−239.
(42) Hori, Y.; Hashimoto, T.; Wakutani, Y.; Urakami, K.; Nakashima, K.; Condron, M. M.; Tsubuki, S.; Saido, T. C.; Teplow, D. B.; Iwatsubo, T. The Tottori (D7N) and English (H6R) Familial Alzheimer Disease Mutations Accelerate Aβ Fibril Formation without Inscreasing Protofibril Formation. *J. Bio. Chem.* **2007**, *282*, 4916−4923.
(43) Chen, W. T.; Hong, C. J.; Lin, Y. T.; Chang, W. H.; Huang, H. T.; Liao, J. Y.; Chang, Y. J.; Hsieh, Y. F.; Cheng, C. Y.; Liu, H. C.; Chen, Y. R.; Cheng, I. H. Amyloid-Beta (Aβ) D7H Mutation Increases Oligomeric A beta 42 and Alters Properties of A beta-Zinc/Copper Assemblies. *PLoS One* **2012**, *7*, e35807.
(44) Wakutani, Y.; Watanabe, K.; Adachi, Y.; Wada-Isoe, K.; Urakami, K.; Ninomiya, H.; Saido, T. C.; Hashimoto, T.; Iwatsubo, I.; Nakashima, K. Novel Amyloid Precursor Protein Gene Missense Mutation (D678N) in Probable Familial Alzheimer's Disease. *J. Neurol. Neurosurg. Psychiatry* **2004**, *75*, 1039−1042.

(45) Ono, K.; Condron, M. M.; Teplow, D. B. Effects of the English (H6R) and Tottori (D7N) Familial Alzheimer Disease Mutations on Amyloid β-protein Assembly and Toxicity. *J. Bio. Chem.* **2010**, *285*, 23186−23197.
(46) Fede, G. D.; Catania, M.; Morbin, M.; Rossi, G.; Suardi, S.; Mazzoleni, G.; Merlin, M.; Giovagnoli, A. R.; Prioni, S.; Erbetta, A.; et al. Recessive Mutation in the APP Gene with Dominant-Negative Effect on Amyloidogenesis. *Science* **2009**, *323*, 1473−1477.
(47) Lv, Z. J.; Roychaudhuri, R.; Condron, M. M.; Teplow, D. B.; Lyubchenko, Y. L. Mechanism of Amyloid β-protein Dimerization Determined Using Single-molecule AFM Force Spectroscopy. *Sci. Rep.* **2013**, *3*, srep02880.
(48) Geyer, C. J. Markov Chain Monte Carlo Maximum Likelihood. Proceedings of*23rd Symposium on the Interface between Computing Science and Statistics - Critical Applications of Scientific Computing: Biology, Engineering, Medicine, Speech*, 1991, Interface Foundation North America: Fairfax, Seattle, WA; p 156.
(49) Hukushima, K.; Nemoto, K. Exchange Monte Carlo Method and Application to Spin Glass Simulations. *J. Phys. Soc. Jpn.* **1996**, *65*, 1604−1608.
(50) Hansmann, U. H. E. Parallel Tempering Algorithm for Conformational Studies of Biological Molecules. *Chem. Phys. Lett.* **1997**, *281*, 140−150.
(51) Sugita, Y.; Okamoto, Y. Replica-exchange Molecular Dynamics Method for Protein Folding. *Chem. Phys. Lett.* **1999**, *314*, 141−151.
(52) Nguyen, P. H.; Tarus, B.; Derreumaux, P. Familial Alzheimer A2V Mutation Reduces the Intrinsic Disorder and Completely Changes the Free Energy Landscape of the Aβ_{1-28} Monomer. *J. Phys. Chem. B* **2013**, *118*, 501−510.
(53) Viet, M. H.; Nguyen, P. H.; Ngo, S. T.; Li, M. S.; Derreumaux, P. Effect of the Tottori Familial Disease Mutation (D7N) on the Monomers and Dimers of Aβ40 and Aβ42. *ACS Chem. Neurosci.* **2013**, *4*, 1446−1457.
(54) Viet, M. H.; Nguyen, P. H.; Derreumaux, P.; Li, M. S. Effect of the English Familial Disease Mutation (H6R) on the Monomers and Dimers of Aβ40 and Aβ42. *ACS Chem. Neurosci.* **2014**, DOI: 10.1021/cn500007j.
(55) Jorgensen, W. L.; Maxwell, D. S.; Tirado-Rives, J. Development and Testing of the OPLS All-atom Force Field on Conformational Energetics and Properties of Organic Liquids. *J. Am. Chem. Soc.* **1996**, *118*, 11225−11236.
(56) Kaminski, G. A.; Friesner, R. A. Evaluation and Reparametrization of the OPSL-AA Force Field for Proteins via Comparison with Accurate Quantum Chemical Calculations on Peptides. *J. Phys. Chem. B* **2001**, *105*, 6474−6487.
(57) Jorgensen, J. W.; Chandrasekhar, J.; Madura, J. D.; Imprey, R. W.; Klein, M. L. Comparison of Simple Potential Functions for Simulating Liquid Water. *J. Chem. Phys.* **1983**, *79*, 926.
(58) Coles, M.; Bicknell, W.; Watson, A. A.; Fairlie, D. P.; Craik, D. J. Solution structure of amyloid β-peptide(1−40) in a water−micelle environment. Is the membrane-spanning domain where we think it is? *Biochemistry* **1998**, *37*, 11064−11077.
(59) Tomaselli, S.; Esposito, V.; Vangone, P.; van Nuland, N. A.; Bonvin, A. M.; Guerrini, R.; Tancredi, T.; Temussi, P. A.; Picone, D. The α-to-β Conformational Transition of Alzheimer's Aβ-(1−42) Peptide in Aqueous Media is Reversible: A Step by Step Conformational Analysis Suggests the Location of β Conformation Seeding. *ChemBioChem* **2006**, *7*, 257−267.
(60) *PyMOL: The PyMOL Molecular Graphics System*, version 1.3; Schrödinger, LLC.
(61) Hess, B.; Kutzner, C.; van der Spoel, D.; Lindahl, E. Gromacs 4: Algorithms for Highly Efficient, Load-Balanced, and Scalable Molecular Simulation. *J. Chem. Theory Comput.* **2008**, *4*, 435−447.
(62) Onufriev, A.; Bashford, D.; Case, D. A. Exploring Protein Native States and Large-scale Conformational Changes with a Modified Generalized Born Model. *Proteins: Struct., Funct., Bioinf.* **2004**, *55*, 383−394.
(63) Sgourakis, N. G.; Yan, Y. L.; McCallum, S. A.; Wang, C. Y.; Garcia, A. E. The Alzheimer's Peptides Aβ40 and 42 Adopt Distinct Conformations in Water: A Combined MD/NMR Study. *J. Mol. Biol.* **2007**, *368*, 1448−1457.
(64) Nguyen, P. H.; Derreumaux, P.; Li, M. S. Effects of All-atom Force Fields on Amyloid Oligomerization: Replica Exchange Molecular Dynamics Simulations of the Aβ_{16-22} Dimer and Trimer. *Phys. Chem. Chem. Phys.* **2011**, *13*, 9778.
(65) Reddy, G.; Straub, J. E.; Thirumalai, D. Influence of Preformed Asp23−Lys28 Salt Bridge on the Conformational Fluctuations of Monomers and Dimers of Aβ Peptides with Implications for Rates of Fibril Formation. *J. Phys. Chem. B* **2009**, *113*, 1162−1172.
(66) Hockney, R. W.; Goel, S. P.; Eastwood, J. Quit High Resolution Computer Models of Plasma. *J. Comput. Phys.* **1974**, *14*, 148−158.
(67) Hess, B.; Bekker, H.; Berendsen, H. J. C.; Fraaije, J. G. E. M. LINCS: A Linear Constraint Solver for Molecular Simulations. *J. Comput. Chem.* **1997**, *18*, 1463−1472.
(68) Bussi, G.; Donadio, D.; Parrinello, M. Canonical Sampling Through Velocity Rescaling. *J. Chem. Phys.* **2007**, *126*, 014101.
(69) Darden, T.; York, D.; Pedersen, L. Particle Mesh Ewald: An $N\cdot\log(N)$ Method for Ewald Sums in Large Systems. *J. Chem. Phys.* **1993**, *98*, 10089−10092.
(70) Patriksson, A.; van der Spoel, D. A Temperature Predictor for Parallel Tempering Simulations. *Phys. Chem. Chem. Phys.* **2008**, *10*, 2073−2077.
(71) Temperature generator for REMD-simulations. http://folding.bmc.uu.se/remd/.
(72) Frishman, D.; Argos, P. Knowledge-Based Protein Secondary Structure Assignment. *Proteins* **1995**, *23*, 566−579.
(73) Heinig, M.; Frishman, D. STRIDE: A Web Server for Secondary Structure Assignment from Known Atomic Coordinates of Proteins. *Nucleic Acids Res.* **2004**, *32*, W500−2.
(74) Mu, Y.; Nguyen, P. H.; Stock, G. Energy Landscape of a Small Peptide Revealed by Dihedral Angle Principal Component Analysis. *Proteins* **2005**, *58*, 45−52.
(75) Mesleh, M. F.; Hunter, J. M.; Shvartsburg, A. A.; Schatz, G. C.; Jarrold, M. F. Structural Information from Ion Mobility Measurements: Effects of the Long Range Potential. *J. Phys. Chem.* **1996**, *100*, 16082.
(76) Chong, S.-H.; Ham, S. Atomic-level Investigations on the Amyloid-β Dimerization Process and its Driving Forces in Water. *Phys. Chem. Chem. Phys.* **2012**, *14*, 1573−1575.
(77) Zhang, S.; Iwata, K.; Lachenmann, M. J.; Peng, J. W.; Li, S.; Stimson, E. R.; Lu, Y.; Felix, A. M.; Maggio, J. E.; Lee, J. P. The Alzheimer's Peptide Aβ Adopts a Collapsed Coil Structure in Water. *J. Struct. Biol.* **2000**, *130*, 130−141.
(78) Danielsson, J.; Jarvet, J.; Damberg, P.; Graslund, A. The Alzheimer β-peptide Shows Temperature-dependent Transitions Between Left-handed 3_1-helix, β-strand and Random Coil Secondary Structures. *FEBS J.* **2005**, *227*, 3938−3949.
(79) Kirkitadze, M. D.; Condron, M. M.; Teplow, D. B. Identification and Characterization of Key Kinetic Intermediates in Amyloid β-protein Fibrillogenesis. *J. Mol. Biol.* **2001**, *312*, 1103−1119.
(80) Ono, K.; Condron, M. M.; Teplow, D. B. Structure Neurotoxicity Relationships of Amyloid β-protein Oligomers. *Proc. Natl. Acad. Sci. U.S.A.* **2009**, *106*, 14745−14750.
(81) Barz, B.; Urbanc, B. Dimer Formation Enhances Structural Differences Between Amyloid β-protein (1−40) and (1−42): An Explicit-solvent Molecular Dynamics Study. *PLoS One* **2012**, *7*, e34345.
(82) Rojas, A.; Liwo, A.; Browne, D.; Scheraga, H. A. Mechanism of Fiber Assembly: Treatment of Aβ Peptide Aggregation with a Coarse-Grained United-Residue Force Field. *J. Mol. Biol.* **2010**, *404*, 537−552.
(83) Viet, M. H.; Li, M. S. Amyloid Peptide Aβ_{40} Inhibits Aggregation of Aβ_{42}: Evidence from Molecular Dynamics Simulations. *J. Chem. Phys.* **2012**, *136*, 245105.
(84) Yang, M.; Teplow, D. B. Amyloid β-protein Monomer Folding: Free Energy Surfaces Reveal Alloform-specific Differences. *J. Mol. Biol.* **2008**, *384*, 450−464.
(85) Rosenman, D. J.; Connors, C.; Chen, W.; Wang, C.; Garcia, A. E. Aβ Monomers Transiently Sample Oligomer and Fibril-like

Configurations: Ensemble Characterization Using a Combined MD/NMR Approach. *J. Mol. Biol.* **2013**, *425*, 3338−3359.
(86) Meral, D.; Urbanc, B. Discrete Molecular Dynamics Study of Oligomer Formation by N-Terminally Truncated Amyloid β-Protein. *J. Mol. Biol.* **2013**, *425*, 2260−2275.
(87) Li, M. S.; Co, N. T.; Hu, C. K.; Straub, J. E.; Thirumalai, D. Determination of Factors Governing Fibrillogenesis of Polypeptide Chains Using Lattice Models. *Phys. Rev. Lett.* **2010**, *105*, 218101.
(88) Lam, A. R.; Teplow, D. B.; Stanley, H. E.; Urbanc, B. Effects of the Arctic ($E^{22}\rightarrow G$) Mutation on Amyloid β-Protein Folding: Discrete Molecular Dynamics Study. *J. Am. Chem. Soc.* **2008**, *130*, 17413−17422.
(89) Viet, M. H.; Ngo, S. T.; Lam, N. S.; Li, M. S. Inhibition of Aggregation of Amyloid Peptides by Beta-Sheet Breaker Peptides and Their Binding Affinity. *J. Phys. Chem. B* **2011**, *115*, 7433−7446.
(90) Snyder, S. W.; Lardor, U. S.; Wade, W. S.; Wang, G. T.; Barrett, L. W.; Matayoshi, E. D.; Huffaker, H. J.; Kraff, G. A.; Holzman, T. F. Amyloid-β Aggregation: Selective Inhibition of Aggregation in Mixtures of Amyloid with Different Chain Lengths. *Biophys. J.* **1994**, *67*, 1216−1228.
(91) Ball, K. A.; Phillips, A. H.; Wemmer, D. E.; Head-Gordon, T. Differences in β-strand Populations of Monomeric Aβ40 and Aβ42. *Biophys. J.* **2013**, *104*, 2714−2724.
(92) Han, M.; Hansmann, U. H. E. Replica Exchange Molecular Dynamics of the Thermodynamics of Fibril Growth of Alzheimer's $A\beta_{42}$ Peptide. *J. Chem. Phys.* **2011**, *135*, 065101.
(93) Velez-Vega, C.; Escobedo, F. A. Characterizing the Structural Behavior of Selected Aβ-42 Monomers with Different Solubilities. *J. Phys. Chem. B* **2011**, *115*, 4900−4910.
(94) Irback, A.; Mohanty, S. Folding Thermodynamics of Peptides. *Biophys. J.* **2005**, *88*, 1560−1569.
(95) Sgourakis, N. G.; Merced-Serrano, M.; Boutsidis, C.; Drineas, P.; Du, Z. M.; Wang, C. Y.; Garcia, A. E. Atomic-level Characterization of the Ensemble of the A β(1−42) Monomer in Water Using Unbiased Molecular Dynamics Simulations and Spectral Algorithms. *J. Mol. Biol.* **2011**, *405*, 570−583.
(96) Gessel, M. M.; Bernstein, S.; Kemper, M.; Teplow, D. B.; Bowers, M. T. Familial Alzheimer's Disease Mutations Differentially Alter Amyloid β-protein Oligomerization. *ACS Chem. Neurosci.* **2012**, *3*, 909−918.
(97) Baumketner, A.; Bernstein, S. L.; Wyttenbach, T.; Bitan, G.; Teplow, D. B.; Bowers, M. T.; Shea, J. E. Amyloid β-protein Monomer Structure: A Computational and Experimental Study. *Protein Sci.* **2006**, *15*, 420−428.
(98) Sciarretta, K. L.; Gordon, D. J.; Petkova, A. T.; Tycko, R.; Meredith, S. C. Aβ 40-Lactam(D23/K28) Models a Conformation Highly Favorable for Nucleation of Amyloid. *Biochemistry* **2005**, *44*, 6003−6014.
(99) Maji, S. K.; Loo, R. R. O.; Inayathullah, M.; Spring, S. M.; Vollers, S. S.; Condron, M. M.; Bitan, G.; Loo, J. A.; Teplow, D. B. Amino Acid Position-specific Contributions to Amyloid β-Protein Oligomerization. *J. Biol. Chem.* **2009**, *284*, 23580−23591.
(100) Jorgensen, W. L.; Madura, J. D. Temperature and Size Dependence for Monte-Carlo Simulations of TIP4P Water. *Mol. Phys.* **1985**, *56*, 1381−1392.
(101) van Gunsteren, W. F.; Billeter, S. R.; Eising, A. A.; Hunenberger, P. H.; Kruger, P.; Mark, A. E.; Scott, W. R. P.; Tironi, I. G. *Biomolecular Simulation: The GROMOS96 Manual and User Guide*; Vdf Hochschulverlag AG an der ETH Zurich: Zurich, 1996.
(102) Nguyen, T. T.; Viet, M. H.; Li, M. S. Effects of Water Models on Binding Affinity: Evidence from All-atom Simulation of Binding of Tamiflu to A/H5N1 Neuraminidase. *Sci. World J.* **2014**, *2014*, 536084.
(103) Mitternacht, S.; Staneva, I.; Hard, T.; Irback, A. Monte Carlo Study of the Formation and Conformational Properties of Dimers of Aβ42 Variants. *J. Mol. Biol.* **2011**, *410*, 357−367.
(104) Zhang, T.; Zhang, J.; Derreumaux, P.; Mu, Y. Molecular Mechanism of the Inhibition of EGCG on the Alzheimer $A\beta_{1-42}$ Dimer. *J. Phys. Chem. B* **2013**, *117*, 3993−4002.
(105) Cote, S.; Laghaei, R.; Derreumaux, P.; Mousseau, N. Distinct Dimerization for Various Alloforms of the Amyloid-Beta Protein: $A\beta_{1-40}$, $A\beta_{1-42}$, and $A\beta_{1-40}$(D23N). *J. Phys. Chem. B* **2012**, *116*, 4043−4055.